Delft University of Technology

Tensile characterization and constitutive modeling of sintered nano-silver particles over a range of strain rates and temperatures

Qian, Cheng; Gu, Tijian; Wang, Ping; Cai, Wei; Fan, Xuejun; Zhang, Guoqi; Fan, Jiajie

DOI
10.1016/j.microrel.2022.114536

Publication date
2022

Document Version
Final published version

Published in
Microelectronics Reliability

Citation (APA)
Qian, C., Gu, T., Wang, P., Cai, W., Fan, X., Zhang, G., & Fan, J. (2022). Tensile characterization and constitutive modeling of sintered nano-silver particles over a range of strain rates and temperatures. *Microelectronics Reliability*, *132*, 1-8. Article 114536. https://doi.org/10.1016/j.microrel.2022.114536

Important note
To cite this publication, please use the final published version (if applicable).
Please check the document version above.

Copyright
Other than for strictly personal use, it is not permitted to download, forward or distribute the text or part of it, without the consent of the author(s) and/or copyright holder(s), unless the work is under an open content license such as Creative Commons.

Takedown policy
Please contact us and provide details if you believe this document breaches copyrights.
We will remove access to the work immediately and investigate your claim.

This work is downloaded from Delft University of Technology.
For technical reasons the number of authors shown on this cover page is limited to a maximum of 10.

Green Open Access added to TU Delft Institutional Repository

'You share, we take care!' - Taverne project

https://www.openaccess.nl/en/you-share-we-take-care

Otherwise as indicated in the copyright section: the publisher
is the copyright holder of this work and the author uses the
Dutch legislation to make this work public.

Microelectronics Reliability 132 (2022) 114536

Contents lists available at ScienceDirect

Microelectronics Reliability

journal homepage: www.elsevier.com/locate/microrel

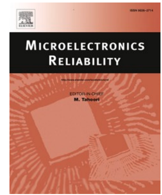

Tensile characterization and constitutive modeling of sintered nano-silver particles over a range of strain rates and temperatures

Cheng Qian [a,b], Tijian Gu [d], Ping Wang [d], Wei Cai [d], Xuejun Fan [f], Guoqi Zhang [e], Jiajie Fan [a,b,c,e,*]

[a] Institute of Future Lighting, Academy for Engineering & Technology, Fudan University, Shanghai 200433, China
[b] Shanghai Engineering Technology Research Center for SiC Power Device, Fudan University, Shanghai 200433, China
[c] Research Institute of Fudan University in Ningbo, Ningbo 315336, China
[d] College of Mechanical and Electrical Engineering, Hohai University, Changzhou 213022, China
[e] EEMCS Faculty, Delft University of Technology, Delft 2628 CD, the Netherlands
[f] Department of Mechanical Engineering, Lamar University, Beaumont, TX 77710, USA

ARTICLE INFO

Keywords:
Power electronics packaging
Nano-silver sintering
Constitutive model
Anand model
Variable-order fractional model

ABSTRACT

Sintered nano-silver die-attach materials have been widely used in high-power electronics packaging because of their high thermal and electrical conductivities. In this study, we characterized the tensile properties of sintered nano-silver particles over a range of strain rates and temperatures, and established the constitutive models. First, 50 nm nano-silver particles were sintered at 275 °C for 50 min as test samples, and their tensile tests were conducted under a dynamic thermomechanical analyzer (DMA Q800) and an IBTC 300SL in-situ mechanical test system respectively with different strain rates and ambient temperatures. Then, both Anand and variable-order fractional models (VoFM) were adopted to analyze the obtained stress-strain data and we studied their fitting accuracy and applicability. The results showed that: (1) The Young's modulus of the sintered nano-silver particles decreased with increasing temperature. In addition, the tensile strengths declined under lower strain rates and higher temperature conditions; (2) both the Anand model and VoFM characterized the tensile stress-strain properties of the sintered nano-silver material well. Compared to the Anand model, the VoFM utilized a simpler formula with fewer parameters and higher precision.

1. Introduction

A new generation of wide-bandgap power electronics has attracted widespread attention due to the development of power electronics, as represented by SiC and GaN [1]. In aerospace, automotive, and other application fields, power devices and modules have to operate in high temperature environments (over 200 °C) with large temperature fluctuations [2]. This places higher requirements on the packaging technology of power electronics. The Restriction of Hazardous Substances law imposed by the European Union restricts the use of lead solder materials and promotes lead-free processes [3–6]. New types of lead-free solder mainly include Sn-Cu, Sn-Ag, Sn-Bi binary solder, and Sn-Ag-Cu ternary alloy solder with a melting point ranging from 183 °C to 221 °C [7,8]. However, these materials easily decompose at high temperatures, making it difficult to meet the electrical conductivity, heat conduction, and heat dissipation requirements for wide-bandgap semiconductor power modules. Compared to traditional lead-free solder, nano-metal particle sintered materials offer better electrical interconnection, mechanical support, and heat dissipation channel properties for wide bandgap semiconductor power electronics packaging, and to achieve the request on low temperatures packaging and high temperatures service [9,10].

The sintered nano-silver has attracted attention in the field of high-power electronics packaging because of their high thermal conductivity, electrical conductivity, and high operating temperature [11–13]. The proposal and promotion of low-temperature joining technology (LTJT) [14] has resulted in the sintering temperatures of nano-silver pastes dropping below 300 °C. This has also promoted sintering, by reducing the particle sizes of the nano-silver particles [15]. Zhang and Lu [16] developed a pressure-assisted sintering process using micron-scale silver paste sintering method to package power devices, obtaining reliable interconnections. Bai et al. [17] prepared sintered nano-

* Corresponding author at: Institute of Future Lighting, Academy for Engineering & Technology, Fudan University, Shanghai 200433, China.
E-mail address: jiajie_fan@fudan.edu.cn (J. Fan).

https://doi.org/10.1016/j.microrel.2022.114536
Received 7 November 2021; Received in revised form 11 March 2022; Accepted 4 April 2022
Available online 10 April 2022
0026-2714/© 2022 Elsevier Ltd. All rights reserved.

silver samples using low-temperature sintering technology at 280 °C, and their thermal conductivity and conductivity were much higher than traditional solder alloys, with a smaller Young's modulus. Wang et al. [18] studied the low-temperature sintering process of nano-silver materials, and analyzed the effects of sintering temperature, heating rate, and holding time on the sintering process. Under appropriate sintering conditions, the micron/submicron silver particle solder paste also exhibited high joint strength. Mei et al. [19] realized the rapid sintering of micron solder paste by appropriately increasing the sintering pressure and temperature, and the joint strength reached 50 MPa. The reliability of nano-silver paste has also been extensively studied, including indentation hardness, plasticity, ratcheting, and pore ratio properties [20–22]. Chen et al. [23,24] studied the ratchet effects of nano-silver sintered joints using experimental and simulation methods. Li et al. [25] also reported the reliability of sintered silver joints and compared the bending curvatures of sintered silver joints and solder joints over 800 thermal cycles, and the results showed that the sintered silver joints had higher reliability. Sakamoto et al. [26] compared the thermal cycle reliabilities of nano-particle silver paste, micron-flake silver paste, and nano-flake silver paste joints, and the results showed that the strength of the nano-flake silver solder paste joints significantly improved after 250 cycles.

Constitutive modeling is one of important tools for predicting material stress-strain responses and material mechanical failure mechanisms. Currently, the Anand model is the main constitutive model used to describe the mechanical properties of tin-lead and lead-free solders [27]. Previous studies have shown that sintered nano silver materials exhibited viscoplastic mechanical behavior at high temperatures. However, as its viscoplastic property is not noticeable at low temperatures, current constitutive models are still based on the Anand model. For example, Yu et al. [28] described the uniaxial tensile properties of low-temperature sintered nano-silver films using the Anand model. However, the extraction process for nine independent parameters in the Anand model was complicated. Moreover, the fractional calculus is considered as an effective method for establishing complex constitutive models [29]. Specifically, the variable-order fractional model (VoFM) provides a new tool for characterizing the mechanical properties of new materials. When the fractional order is 0, the model can characterize the elastic behavior of the material, and when the fractional order is considered a function of strain or time, it can be used to characterize the viscoplastic behavior of the material [30].

According to the above literature review, there are numerous studies on the joint strength and reliability of sintered nano-silver under different sintering conditions, however, report on its evolution of mechanical properties under different strain rates and ambient temperatures are rare. Considering the above advantages of VoFM, the motivation of this paper is to model the high temperature tensile behavior of sintered nano-silver particles by comparing the VoFM with classical Anand model. The remaining portions of this study are organized as follows: Section 2 introduces the theoretical models, Section 3 describes the sintering process used to prepare the test samples and describes the test process, Section 4 discusses the compared fitting results, and the concluding remarks are given in Section 5.

2. Constitutive modeling

2.1. Variable-order fractional model (VoFM)

The tensile strain of sintered nano-silver particles can be divided into two processes, including the viscoelastic phase and the viscoplastic phase. The formula can be expressed by [30]

$$\varepsilon(t) = \begin{cases} \varepsilon_e(t) & 0 \le t \le t_E \\ \varepsilon_E + \varepsilon_{ev}(t) & t_E \le t \le t_b \end{cases}, \tag{1}$$

where ε_e and ε_{ev} correspond to the linear elastic strain and viscoelastic strain, respectively, t_E represents the time when the linear elastic strain reaches the maximum value ε_E, and t_b represents the failure time. The material exhibits linear elasticity before t_E; therefore, the stress-strain relationship follows Hooke's law:

$$\sigma_e(t) = E\varepsilon_e(t), \tag{2}$$

where E is the Young's modulus.

When the strain rate is constant, the stress and strain in the visco-plastic stage can be expressed by [31]

$$\sigma_{ve}(\mathrm{t}) = \frac{E(c\phi)^{\alpha}\varepsilon^{1-\alpha}}{\Gamma(2-\alpha)}, 0 < \alpha < 1, \tag{3}$$

where c denotes the strain rate and ϕ is a material parameter that is affected by the ambient temperature and strain rate. When the fractional order α for performance is between 0 and 1, then $\Gamma(*)$ is the gamma function, according to

$$\Gamma(z) = \int_0^{\infty} e^{-v} t^{z-1} dv, Re(z). > 0. \tag{4}$$

Also, the expression for the viscoplastic stage during a nonlinear

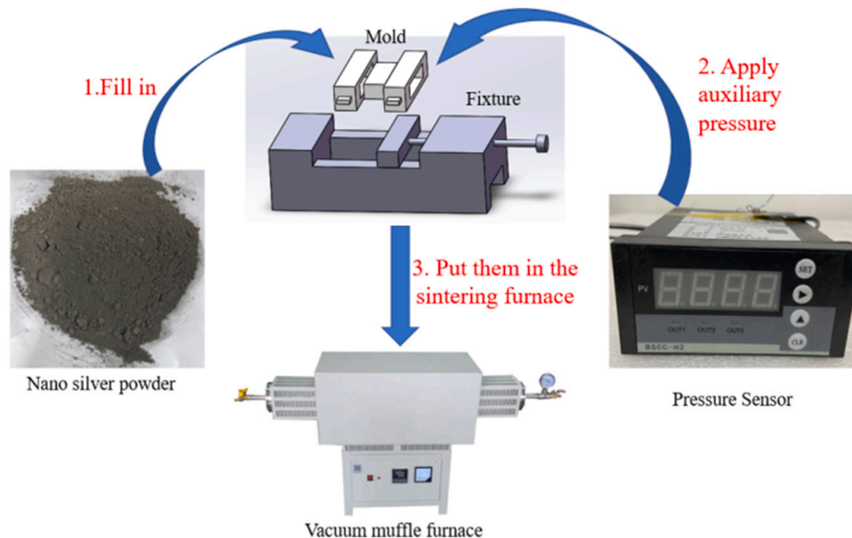

Fig. 1. Test sample preparation process.

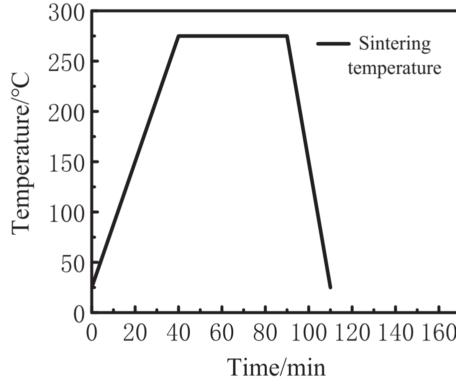

Fig. 2. Sintering temperature curve.

stress response is given by

$$\sigma_{ve}(\mathrm{t}) = \frac{Ec\phi^{\alpha(t)}}{\Gamma(2-\alpha(t))} t^{1-\alpha(t)}, 0 < \alpha(t). < 1. \tag{5}$$

2.2. Anand model

A unified viscoplastic material constitutive model was proposed by Anand and further improved by Brown [27]. The model is expressed by

$$\sigma = cs, \tag{6}$$

where c is a function of temperature and strain rate, and s is an internal variable:

$$c = \frac{1}{\xi} sinh^{-1}\left(\left(\frac{\dot{\varepsilon}_p}{A} e^{\frac{Q}{RT}}\right)^m\right) \quad c < 1, \tag{7}$$

where $\dot{\varepsilon}_{\mathrm{p}}$ is the inelastic strain rate, A is a constant, Q is the activation energy, m is the strain rate sensitivity index, ξ is the stress multiplier, R is the gas constant, and T is the absolute temperature. The internal variable can be expressed by

$$\dot{\mathrm{s}} = \left[h_0 \left|1 - \frac{s}{s^*}\right|^a sign\left(1 - \frac{s}{s^*}\right)\right]\dot{\varepsilon}_p, \tag{8}$$

where

$$\mathrm{s}^* = \widehat{s}\left[\frac{\dot{\varepsilon}_p}{A} exp\left(\frac{Q}{RT}\right)\right]^n. \tag{9}$$

In Eq. (8), S^* represents the saturation value of the internal variables at a given temperature and strain rate, h_0 is the hardening/softening coefficient, and a is the strain rate sensitivity index. In Eq. (9), $\widehat{s}$ and n denote the coefficient and strain rate sensitivity for the saturation value for deformation resistance, respectively.

The flow model adopted by the Anand model can also be expressed by

$$\dot{\varepsilon}_p = Aexp\left(-\frac{Q}{RT}\right)\left[sinh\left(\xi\frac{\sigma}{s}\right)\right]^{1/m}. \tag{10}$$

3. Sample preparation and tests

3.1. Sintering process of nano-silver particles

Fig. 1 shows a schematic of the sample preparation process, where the raw material consisted of nano-silver powder with an average particle size of 50 nm. The quantitative raw materials were weighed and placed in the molds, which were separated by iron blocks and fixed with a clamp. After sample filling was completed, an auxiliary pressure of 30 MPa was applied to the samples using a pressure sensor. Then the jig was placed into a vacuum muffle furnace for sintering, and the sintering curve is shown in Fig. 2. The temperature increased from room temperature to 275 °C at a constant heating rate for 40 min and then maintained for 50 min. Afterward, the sintered nano-silver particles was demolded and cooled to room temperature.

3.2. The tensile test under IBTC 300SL

We prepared the tensile test samples for the IBTC-300SL in-situ mechanical test system according to the following process. First, 0.8 g of raw materials were weighed, and then we obtained a rectangular sheet with a size of 30 * 6 * 0.8 mm using a low-temperature sintering process as shown in Figs. 1 and 2. The sintered nano-silver sheet was then divided to three test samples with a size of 30 * 2 * 0.8 mm through a wire cutting.

Tensile tests on the prepared sample were conducted as shown in Fig. 3. The constant strain rate tensile method was used in the test. In order to ensure the test accuracy, a 300 N sensor was installed on IBTC-300SL in-situ mechanical test system for load collection, and the strain is obtained by displacement measurement and calculation, a temperature control box with a temperature range of room temperature to 400 °C was used to maintain a constant temperature. The testing conditions under IBTC 300SL consisted of three temperatures (60 °C, 120 °C, and 185 °C) and five constant strain rates (0.001%, 0.005%, 0.01%, 0.05%, and 0.1%/s). Three samples were tested under each condition.

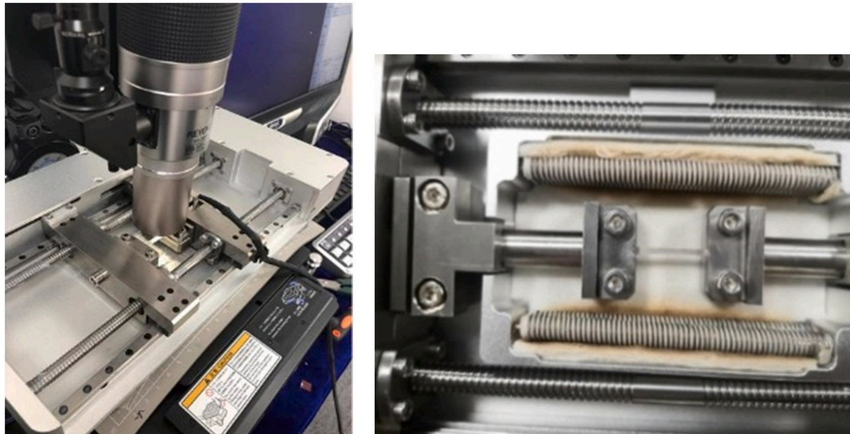

Fig. 3. The IBTC-300SL in-situ mechanical test system.

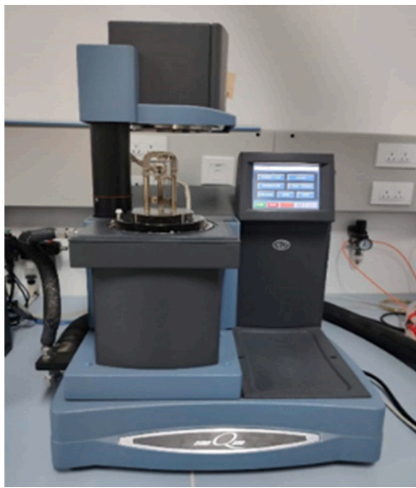

Fig. 4. DMA Q800.

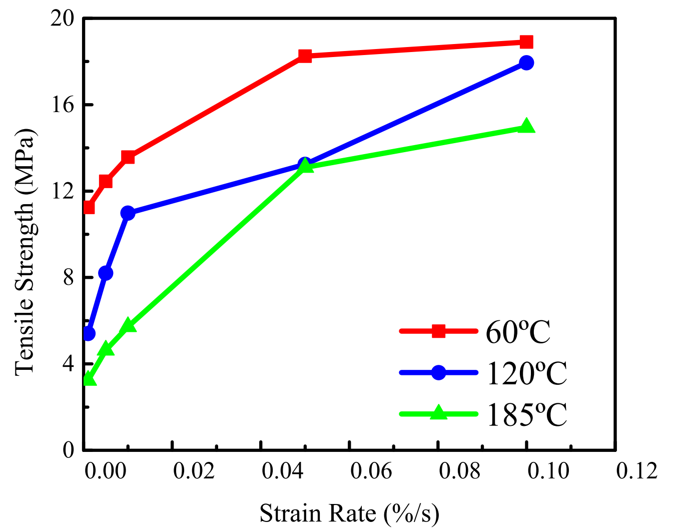

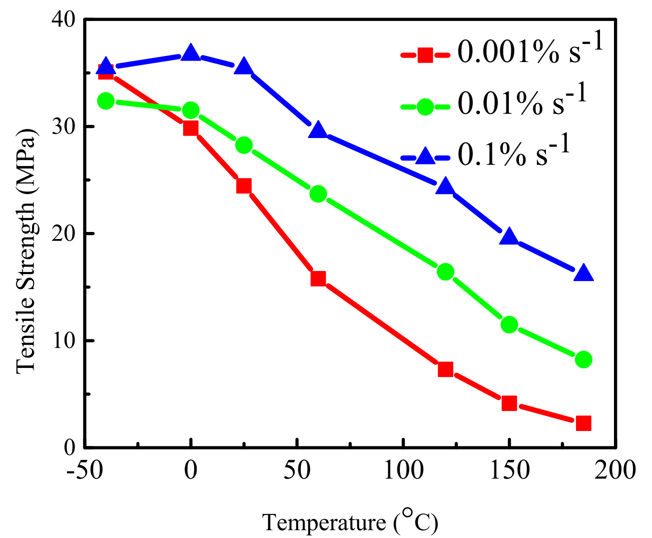

Fig. 6. Tensile strength of the sintered nano-silver particles obtained from (a) the IBTC-300SL and (b) DMA Q800.

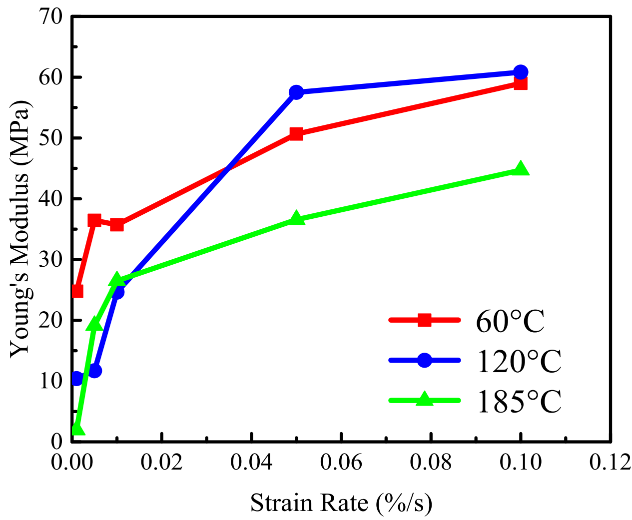

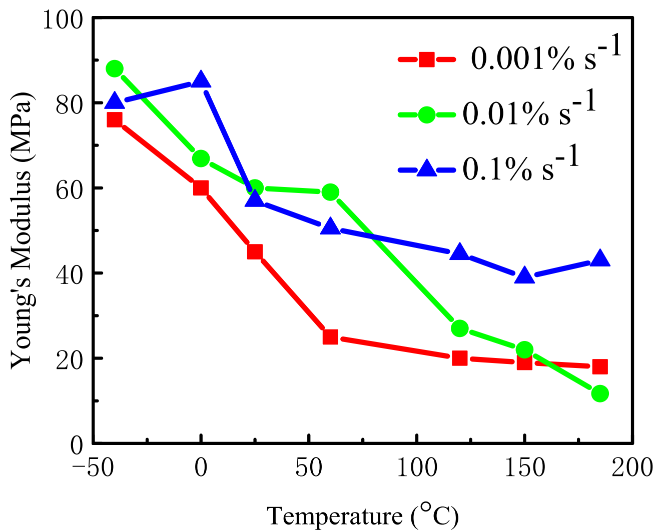

Fig. 5. Young's modulus of the sintered nano-silver particles obtained from (a) the IBTC-300SL and (b) DMA Q800.

3.3. The tensile test under DMA Q800

Another tensile test was performed on a DMA Q800 instrument, as shown in Fig. 4. The test samples with a size of 30 * 2 * 0.3 mm were prepared under the same process as shown in Figs. 1 and 2. The similar tensile test method was adopted under DMA Q800: the force sensor with loading accuracy of 0.00001 N was used for load collection, and the strain was obtained by displacement measurement and calculation, a temperature control box was used to maintain a constant temperature. The testing conditions included three constant strain rates (0.001%, 0.01%, and 0.1%/s) and seven ambient temperatures (−40 °C, 0 °C, 25 °C, 60 °C, 120 °C, 150 °C, and 185 °C). Three samples were tested under each condition.

4. Results and discussion

4.1. Static mechanical properties analysis

The initial linear elastic phases of the stress-strain data for nano-silver sintered samples obtained from the IBTC-300SL in-situ

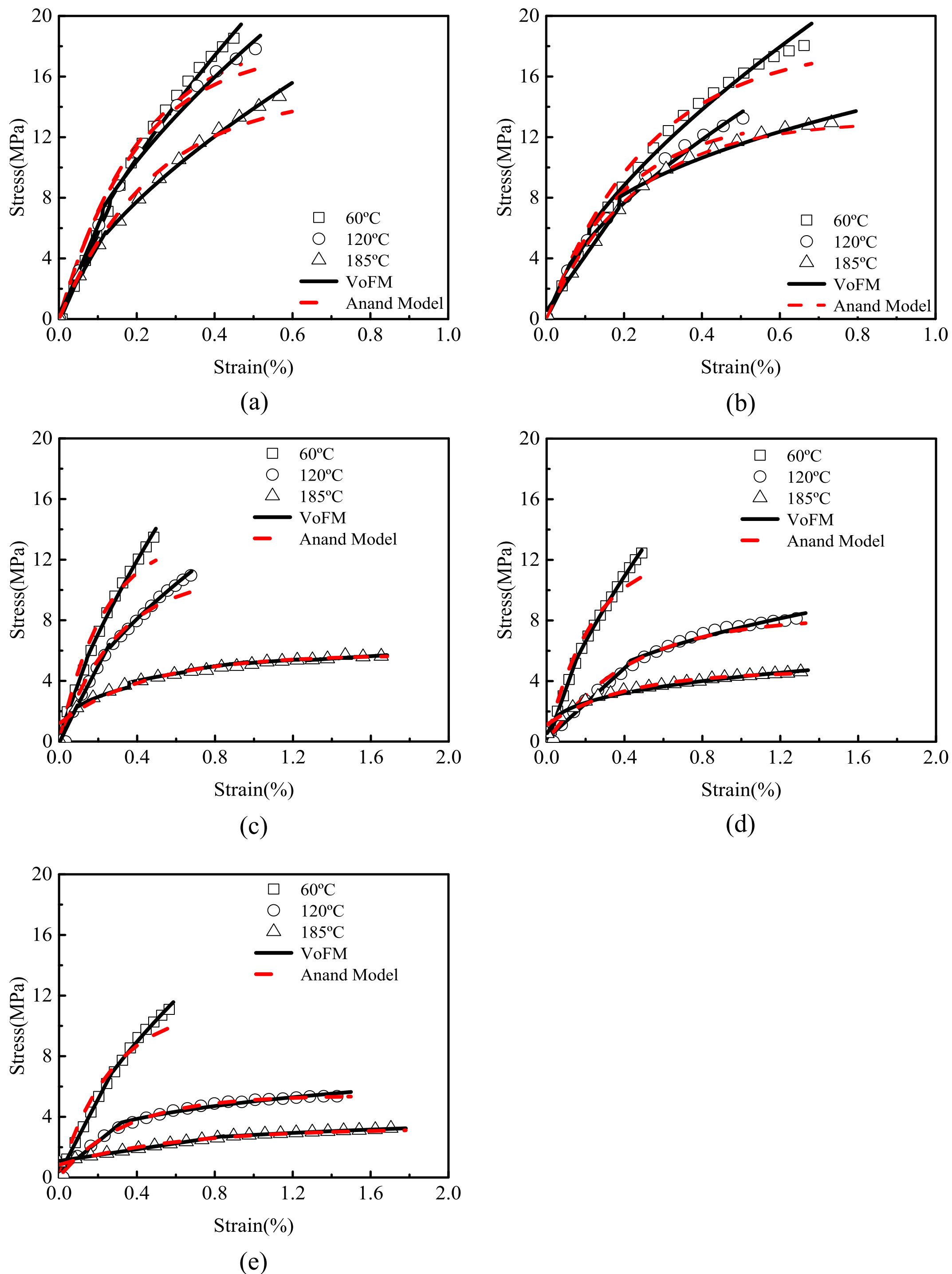

Fig. 7. The fitting results of stress-strain data collected by the IBTC-300SL tensile test (a) 0.1%/s, (b) 0.05%/s, (c) 0.01%/s, (d) 0.005%/s, and (e) 0.0001%/s.

mechanical test system and the DMA Q800 were fitted, and the slopes of the fitted lines were considered as the Young's modulus of the test samples. As shown in Figs. 5 and 6, Whether the tensile tests were conducted under a DMA Q800 or an IBTC 300SL in-situ mechanical test system, the Young's modulus and tensile strength properties of the sintered nano silver particles were simultaneously affected by the temperature and strain rate. The results indicate that: when the temperature was constant, the tensile strength increased as the strain rate increased. When the strain rate was constant, the Young's modulus and tensile strength decreased with increasing temperature.

4.2. *Comparison of fitted results*

As shown in Fig. 7, the stress-strain data of the nano silver sintered samples collected by the IBTC-300SL system were fitted by the Anand model and VoFM. The fitting processing for the stress-strain data from the DMA Q800 tensile test was the same. The fitting results are shown in Fig. 8.

The fitting parameters α_0 for the VoFM are shown in Tables 1 and 2, those reflected the changes in viscoelastic mechanical properties. The fractional order α_0 varies between 0 and 1, which respectively corresponds to pure solid and pure fluid. That means the smaller α_0 indicates

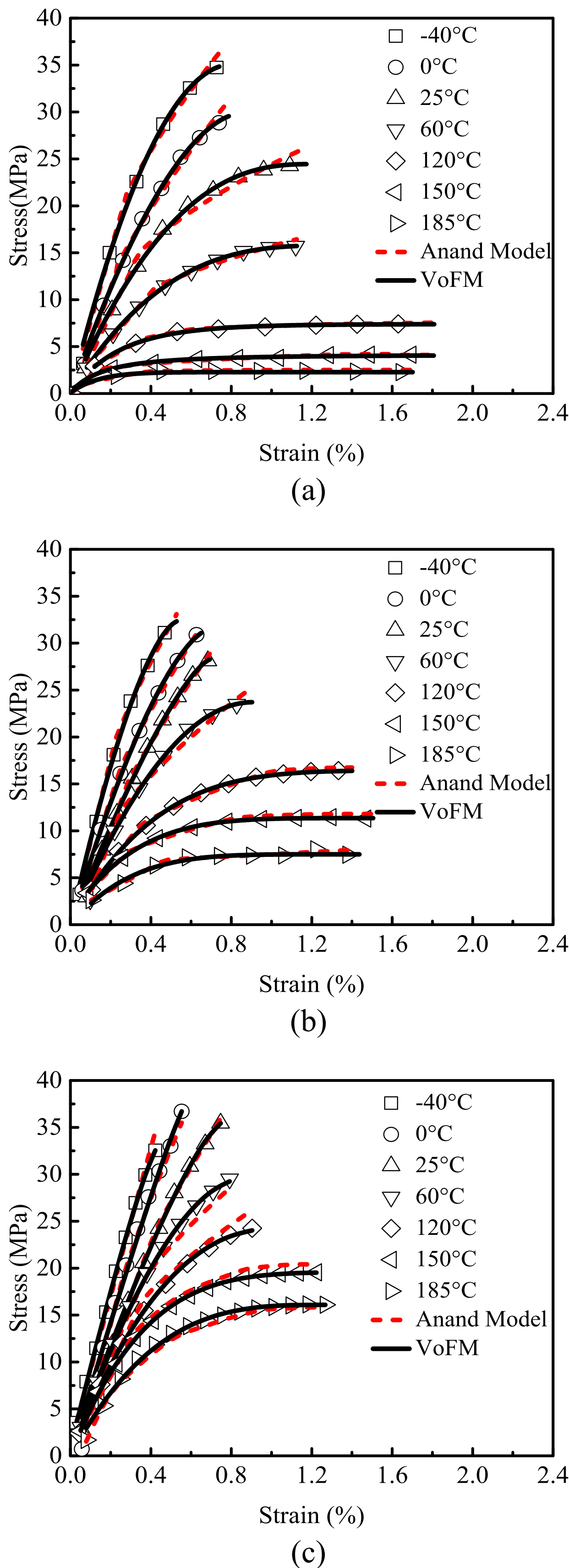

Fig. 8. The fitting results of stress-strain data collected by the DMA Q800 tensile test (a) 0.001%/s, (b) 0.01%/s, (c) 0.1%/s.

Table 1
The fitting parameter α_0 of the VoFM in IBTC-300SL tensile test.

Strain rate	Temperature		
	60 °C	120 °C	185 °C
0.1%/s	0.2876	0.3840	0.3624
0.05%/s	0.3527	0.3719	0.6296
0.01%/s	0.2504	0.3828	0.7569
0.005%/s	0.2728	0.5904	0.6818
0.001%/s	0.3312	0.7140	0.7503

Table 2
The fitting parameter α_0 of the VoFM in DMA Q800 tensile test.

Temperature	Strain rate		
	0.1%/s	0.01%/s	0.001%/s
−40 °C	0	0.3992	0.4492
0 °C	0.2073	0.3229	0.3203
25 °C	0.2875	0.2714	0.5492
60 °C	0.4712	0.4264	0.6197
120 °C	0.4982	0.5932	0.6861
150 °C	0.5493	0.6373	0.7831
185 °C	0.5217	0.8933	0.5102

Table 3
RMSE of the Anand and variable-order fractional modeling on the IBTC-300SL tensile test results.

Temperature	Strain rate	Models	
		Anand	VoFM
60 °C	0.1%/s	1.1246	0.3328
	0.05%/s	0.7327	0.4650
	0.01%/s	0.7670	0.1697
	0.005%/s	0.7093	0.0652
	0.001%/s	0.6826	0.1199
	0.1%/s	0.7581	0.4135
	0.05%/s	0.4938	0.3228
120 °C	0.01%/s	0.5214	0.1572
	0.005%/s	0.2726	0.1892
	0.001%/s	0.0569	0.1296
	0.1%/s	0.5904	0.2294
	0.05%/s	0.2608	0.2629
185 °C	0.01%/s	0.1856	0.0919
	0.005%/s	0.1146	0.0956
	0.001%/s	0.0719	0.0268

greater elasticity and less viscosity. When the fractional order was constant, the constant order α_0 increased with increasing temperature at a constant strain rate. It was due to the softening of the metallic material with increasing temperature. However, under certain conditions, the constant order α_0 was not sufficient to describe the viscoelastic deformation well. When the fractional order was a variable, it appeared as a linear function with respect to time $\alpha(t)$, that presents in the non-linear tensile stage. According to Figs. 7 and 8, and Tables 1 and 2, those are verified the feasibility of the VoFM for characterizing the mechanical properties of sintered nano-silver materials.

For the fitting results of stress-strain data collected by both tensile tests, both the variable-order fractional and Anand models described the stress-strain response of the sintered nano-silver particles well. The Anand model is mainly used to characterize plastic strain, and is not good at describing linear elastic deformation at low temperatures. Comparing the root mean square error (RMSE) of fitting results for both models, shown in Tables 3 and 4, whether it is the linear elastic stage or plastic strain, the fitting accuracy of VoFM was better than the Anand model. Furthermore, the Anand model required more parameters for the fitting process, with a more complicated fitting complexity compared to the VoFM. It can be seen that the VoFM performs better in describing the tensile behavior of sintered nano-silver particles over a wide range of

Table 4
RMSE of the Anand and variable-order fractional modeling on the DMA Q800 tensile test results.

Temperature	Strain rate	Models	
		Anand	VoFM
−45 °C	0.001%/s	0.5652	0.3856
	0.01%/s	0.3581	0.3525
	0.1%/s	0.7569	0.1986
0 °C	0.001%/s	0.5683	0.2526
	0.01%/s	0.3518	0.2144
	0.1%/s	0.7817	1.4089
25 °C	0.001%/s	0.7127	0.3020
	0.01%/s	0.3461	0.3430
	0.1%/s	0.3429	0.2912
60 °C	0.001%/s	0.2856	0.0680
	0.01%/s	0.7096	0.4292
	0.1%/s	0.8710	0.1298
120 °C	0.001%/s	0.0931	0.0823
	0.01%/s	0.2860	0.0567
	0.1%/s	0.6468	0.1199
150 °C	0.001%/s	0.0942	0.0919
	0.01%/s	0.2184	0.0477
	0.1%/s	0.6508	0.0655
185 °C	0.001%/s	0.1050	0.1103
	0.01%/s	0.1002	0.2321
	0.1%/s	0.4479	0.3748

strain rates and temperatures, which provides a new and more effective constitutive modeling of sintered nano-metal particles.

5. Conclusions

In this study, we characterized the tensile behavior of sintered nano-silver particles at different temperatures and strain rates. Then two constitutive models, i.e. Anand model and VoFM, were applied to describe their high-temperature deformation behaviors. After comparing and analyzing the fitted results of tensile tests under both DMA Q800 and IBTC 300SL, the identical concluding remarks can be obtained: first, the Young's modulus of the sintered nano-silver particles decreased with increasing temperature, and the tensile strength decreased with increasing temperature or decreasing strain rate. Furthermore, both Anand model and VoFM represented the tensile properties of the sintered nano-silver well, however, the fitting accuracy of the VoFM was slightly better than the Anand model, especially under low-temperature conditions. Anand model can merely characterize its viscoplastic behavior, while the sintered nano-silver particles always show both viscoelastic and viscoplastic behaviors in the tensile tests under different strain rates and temperatures. The VoFM can characterize these two behaviors simultaneously, which is more versatility. Moreover, compared to the Anand model, the VoFM also offered certain advantages in fewer parameters and a simple fitting process. Generally, the VoFM is an effective method to characterize the mechanical deformation behavior of sintered nano-silver particles over a wide range of strain rates and temperatures.

CRediT authorship contribution statement

Cheng Qian: Investigation, Data curation; Writing—original draft.
Tijian Gu: Experiments and data collection.
Ping Wang: Formal analysis, Validation.
Wei Cai: Formal analysis, Validation.
Xuejun Fan: Supervision.
Guoqi Zhang: Supervision.
Jiajie Fan: Conceptualization; Methodology; Writing—review & editing; Project administration; Funding acquisition.

Declaration of competing interest

All authors declare no conflict of interest.

Acknowledgements

This work was supported by National Natural Science Foundation of China (51805147), Shanghai Pujiang Program (2021PJD002) and Taiyuan Science and Technology Development Funds (Jie Bang Gua Shuai Program).

References

[1] V. Veliadis, The impact of education in accelerating commercialization of wide-bandgap power electronics [expert view], IEEE Power Electron. Mag. 6 (2) (2019) 62–66.
[2] C. Buttay, et al., State of the art of high temperature power electronics, Mater. Sci. Eng. B 176 (4) (2011) 283–288.
[3] R. Tian, C. Hang, Y. Tian, L. Zhao, Growth behavior of intermetallic compounds and early formation of cracks in Sn-3Ag-0.5Cu solder joints under extreme temperature thermal shock, Mater. Sci. Eng. A 709 (2018) 125–133.
[4] W. Zhu, W. Zhang, W. Zhou, P. Wu, Improved microstructure and mechanical properties for SnBi solder alloy by addition of Cr powders, J. Alloys Compd. 789 (2019) 805–813.
[5] Q. Yang, T. Otsuki, E. Michida, Product-related environmental regulation, innovation, and competitiveness: empirical evidence from Malaysian and Vietnamese firms, Int. Econ. J. 34 (3) (2020/07/02 2020.) 510–533.
[6] H. Merdad, M. Renaud, State of legislative and normative art in the fields of the environment, health and security of European electrical and electronic equipment, Eur. J. Electr. Eng. 22 (4–5) (2020) 293–300.
[7] J. Wu, S. Xue, J. Wang, M. Wu, J. Wang, Effects of α-Al2O3 nanoparticles-doped on microstructure and properties of Sn–0.3Ag–0.7Cu low-Ag solder, J. Mater. Sci. Mater. Electron. 29 (9) (2018) 7372–7387.
[8] H.R. Kotadia, P.D. Howes, S.H. Mannan, A review: on the development of low melting temperature Pb-free solders, Microelectron. Reliab. 54 (6–7) (2014) 1253–1273.
[9] Y. Yuan, H. Wu, J. Li, P. Zhu, R. Sun, cu-cu joint formation by low-temperature sintering of self-reducible cu nanoparticle paste under ambient condition, Appl. Surf. Sci. 570 (2021).
[10] J. Yan, et al., Pressureless bonding process using Ag nanoparticle paste for flexible electronics packaging, Scripta Materialia 66 (8) (2012).
[11] C. Qian, et al., Thermal management on IGBT power electronic devices and modules, IEEE Access 6 (2018) 12868–12884.
[12] P. Wang, W. Cai, J. Fan, The temperature-dependent fractional evolutional model for sintered nanoscale silver films, Eur. J. Mech. ASolids 90 (2021).
[13] F. Le Henaff, S. Azzopardi, E. Woirgard, T. Youssef, S. Bontemps, J. Joguet, Lifetime evaluation of nanoscale silver sintered power modules for automotive application based on experiments and finite-element modeling, IEEE Trans. Device Mater. Reliab. 15 (3) (2015) 326–334.
[14] E. Ide, S. Angata, A. Hirose, K. Kobayashi, Metal?metal bonding process using ag metallo-organic nanoparticles, Acta Mater. 53 (8) (2005) 2385–2393.
[15] R. Amro, Low-temperature joining technique as interconnection technology for power electronics, Adv. Mater. Res. 1393 (2011).
[16] Z. Zhang, L. Guo-Quan, Pressure-assisted low-temperature sintering of silver paste as an alternative die-attach solution to solder reflow, IEEE Trans. Electron. Packag. Manuf. 25 (4) (2002) 279–283.
[17] J.G. Bai, Z.Z. Zhang, J.N. Calata, G.Q. Lu, Low-temperature sintered nanoscale silver as a novel semiconductor device-metallized substrate interconnect material, IEEE Trans. Compon. Packag. Technol. 29 (3) (2006) 589–593.
[18] T. Wang, X. Chen, G.-Q. Lu, G.-Y. Lei, Low-temperature sintering with nano-silver paste in die-attached interconnection, J. Electron. Mater. 36 (10) (2007) 1333–1340.
[19] Y. Mei, L. Li, X. Li, W. Li, H. Yan, Y. Xie, Electric-current-assisted sintering of nanosilver paste for copper bonding, J. Mater. Sci. Mater. Electron. 28 (12) (2017) 9155–9166.
[20] H. Zhang, Y. Liu, L. Wang, F. Sun, X. Fan, G. Zhang, Indentation hardness, plasticity and initial creep properties of nanosilver sintered joint, Results Phys. 12 (2019) 712–717.
[21] X. Chen, D.-H. Yu, K.S. Kim, Experimental study on ratcheting behavior of eutectic tin–lead solder under multiaxial loading, Mater. Sci. Eng. A 406 (1–2) (2005) 86–94.
[22] K. Qi, X. Chen, G.Q. Lu, Effect of interconnection area on shear strength of sintered joint with nano-silver paste, Soldering Surf. Mount Technol. 20 (1) (2008) 8–12.
[23] G. Chen, L. Yu, Y.-H. Mei, X. Li, X. Chen, G.-Q. Lu, Reliability comparison between SAC305 joint and sintered nanosilver joint at high temperatures for power electronic packaging, J. Mater. Process. Technol. 214 (9) (2014) 1900–1908.
[24] G. Chen, Z.-S. Zhang, Y.-H. Mei, X. Li, G.-Q. Lu, X. Chen, Ratcheting behavior of sandwiched assembly joined by sintered nanosilver for power electronics packaging, Microelectron. Reliab. 53 (4) (2013) 645–651.
[25] Y. Tan, X. Li, X. Chen, Fatigue and dwell-fatigue behavior of nano-silver sintered lap-shear joint at elevated temperature, Microelectron. Reliab. 54 (3) (2014) 648–653.

[26] S. Sakamoto, T. Sugahara, K. Suganuma, Microstructural stability of Ag sinter joining in thermal cycling, J. Mater. Sci. Mater. Electron. 24 (4) (2012) 1332–1340.

[27] AL, Constitutive equations for the rate-dependent deformation of metals at elevated temperatures, J. Eng. Mater. Technol. 104 (1) (1982).

[28] D.-J. Yu, X. Chen, G. Chen, G.-Q. Lu, Z.-Q. Wang, Applying Anand model to low-temperature sintered nanoscale silver paste chip attachment, Mater. Des. 30 (10) (2009) 4574–4579.

[29] W. Cai, W. Chen, J. Fang, S. Holm, A survey on fractional derivative modeling of power-law frequency-dependent viscous dissipative and scattering attenuation in acoustic wave propagation, Applied Mechanics Reviews 70 (3) (2018).

[30] W. Cai, P. Wang, J. Fan, A variable-order fractional model of tensile and shear behaviors for sintered nano-silver paste used in high power electronics, Mech. Mater. 145 (2020).

[31] I. Podlubny, Fractional differential equations: an introduction to fractional derivatives, fractional differential equations, to methods of their solution and some of their applications, Math. Sci. Eng. 198 (1999) 01/01.